RESEARCH ARTICLE

NANO · MICRO small
www.small-journal.com

Breaking the Temperature Limit of Lithium-Ion Batteries With Carbon Nanotube-Based Electrodes and "Constructive Alliance" Electrolyte Strategy

Zixin Hong, Hui Tian, Zhenhan Fang, Yufeng Luo,* Hengcai Wu, Fei Zhao, Wei Yu, Changhong Liu, Qunqing Li, Shoushan Fan, and Jiaping Wang**

Lithium-ion batteries (LIBs) are paramount in energy storage in consumer electronics and electric vehicles. However, a narrow operating temperature range severely constrains their evolution. In this study, a wide-temperature operating LIB system is constructed utilizing carbon nanotube (CNT)-based electrodes and a "constructive alliance" electrolyte. The unique microstructure of the CNT current collector, with high electrical and thermal conductivity, accelerates the reaction kinetics of active materials at subzero temperatures and optimizes the thermal management of the entire electrode at elevated temperatures. Furthermore, a strategy employing the "constructive alliance" electrolyte is proposed, demonstrating that a simple combination of commercially available electrolytes can enhance resilience to harsh thermal conditions. Molecular dynamics simulations and density functional theory calculations reveal that the hybrid electrolyte predominantly adopts aggregate solvation structures and possesses low Li^+ desolvation barriers regardless of thermal variations. Consequently, the assembled $Li_4Ti_5O_{12}$//$LiCoO_2$ full cell, with a negative/positive electrode material ratio of 1.2, exhibits outstanding electrochemical performance in the wide temperature range of −40 and 60 °C. This innovative strategy overcomes challenges in wide-temperature electrolyte research and offers promise for next-generation wide-temperature LIBs.

1. Introduction

Lithium-ion batteries (LIBs) play a pivotal role in the realm of energy storage due to their remarkable energy densities and extended cycling capabilities, with successful applications in portable electronic devices, electric vehicles, and space exploration.[1] A typical commercial LIB system comprises "slurry-coating" electrodes and carbonate-based electrolytes.[2–6] However, this system presents significant challenges under extreme temperature conditions. In frigid conditions (**Figure 1a**), the polymer binder in the electrodes experiences reduced molecular chain mobility,[7] leading to sluggish kinetics with decelerated diffusion of Li ions and electrons in active materials, especially the anode materials.[8,9] Meanwhile, the activation energy of the Li ion desolvation process at the electrode/electrolyte interface becomes larger,[9,10] and the Li ion transport in the electrolyte is also impeded.[11] In addition, high temperatures can introduce many obstacles though they can accelerate diffusion dynamics. The volatile and flammable organic solvents in the carbonate-based electrolyte are the main cause of fires and explosions. The commonly used $LiPF_6$ salt is prone to decompose into LiF and PF_5^- at high temperatures, which can further react with residual moisture to form HF. Then the generated HF can compromise the structural integrity of electrodes, corrode current collectors, and lead to the dissolution of transition metal ions in the cathode, eventually reducing the coulombic efficiency of the battery.[12–14] The polymer binder also suffers from inadequate thermal dissipation and stability at elevated temperatures.[15–18] Typically, the melting temperature for prevalent polyvinylidene fluoride (PVDF) binder is 167 °C (Figure S1, Supporting Information).[19,20] These inherent shortcomings can trigger heat localization and uncontrolled exothermic reactions within the electrodes, resulting in increased battery temperature and the potential for thermal runaway.[21]

To improve the adaptability of LIBs over wide temperature ranges, refinements can be applied to both the electrode and electrolyte to improve low-temperature kinetics and reinforce high-temperature resilience. Contemporary strategies for electrode

Z. Hong, H. Tian, Z. Fang, H. Wu, F. Zhao, C. Liu, Q. Li, S. Fan, J. Wang
Department of Physics and Tsinghua-Foxconn Nanotechnology Research Center
Tsinghua University
Beijing 100084, China
E-mail: fang_zhenhan@126.com; jpwang@tsinghua.edu.cn

Y. Luo
Department of Applied Biology and Chemical Technology
Faculty of Science
The Hong Kong Polytechnic University
Hong Kong, China
E-mail: yufeng.luo@polyu.edu.hk

W. Yu
School of Mechanical Engineering
Hebei University of Technology
Tianjin 300401, China

Q. Li, J. Wang
Frontier Science Center for Quantum Information
Beijing 100084, China

The ORCID identification number(s) for the author(s) of this article can be found under https://doi.org/10.1002/smll.202401735

DOI: 10.1002/smll.202401735

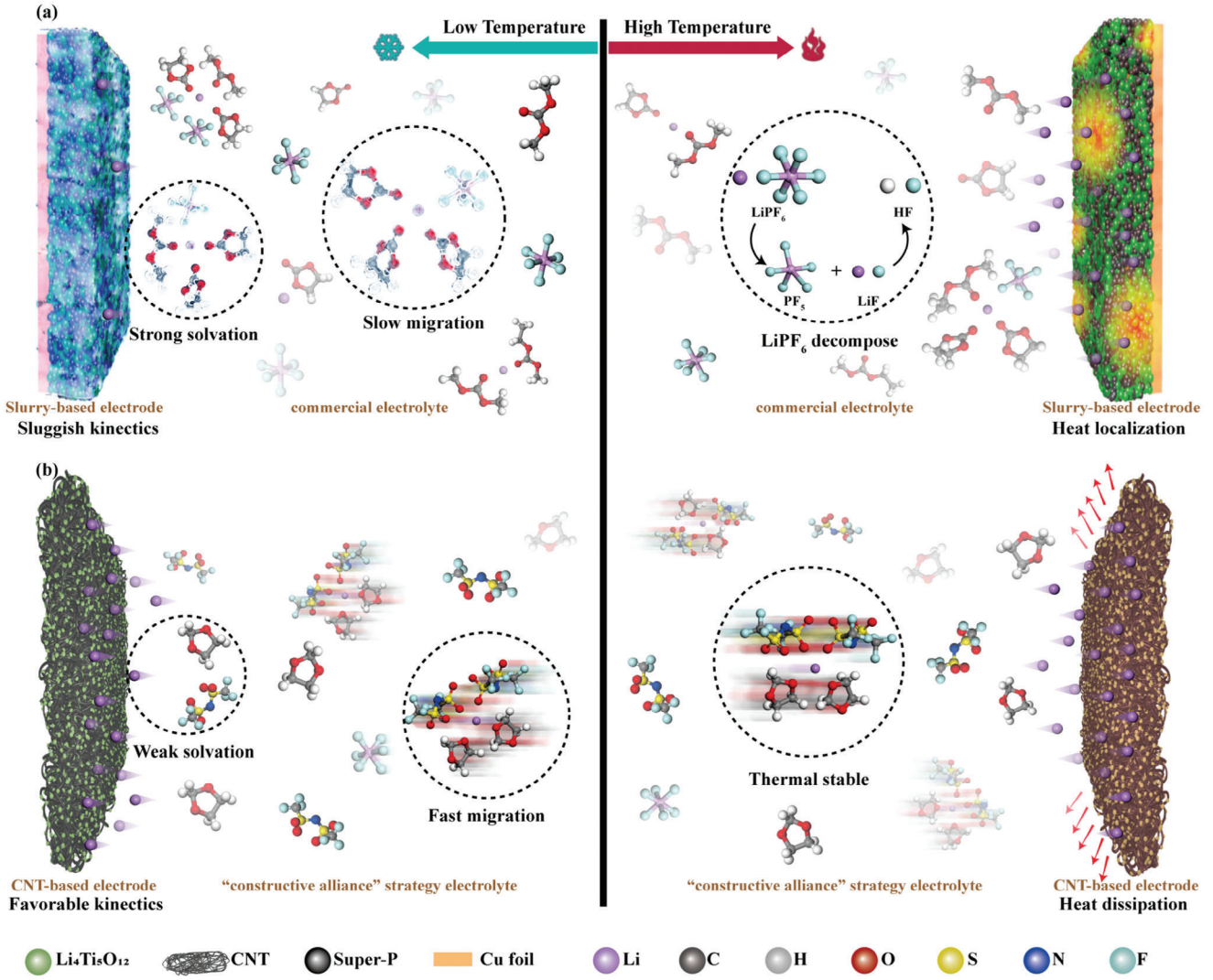

Figure 1. Schematics of a) slurry-based electrodes in conjunction with commercial electrolytes and b) CNT-based electrodes in conjunction with "constructive alliance" strategy electrolytes at low and high temperatures.

modifications include integrating electrode materials with thermal and structural stability (such as $Li_4Ti_5O_{12}$ (LTO)),[22] nano-engineering active materials,[23] elemental doping,[24,25] and designing artificial interfacial layers.[26,27] For instance, Kun et al., successfully incorporated zinc oxide nanoparticles into the expanded graphite, significantly improving lithium ion diffusion kinetics and enabling electrode operation between −50 and 20 °C.[28] Liang et al., co-doped $Li_3V_2(PO_4)_3$ cathode material with Ru and Cl elements, which reduced the energy bandgap and Li^+ diffusion barriers, thereby achieving specific capacities of 49, 128, and 123 mAh g^{-1} at −40, 25, and 60 °C, respectively.[29] However, these methods fail to address the challenges posed by polymer binders in "slurry-coating" electrodes at extreme temperatures. In the realm of wide-temperature electrolytes, most works focus on either high-temperature or low-temperature issues individually.[30] Although several approaches have been proposed to enable LIB operation across the full temperature spectrum, such as the exploration of novel materials,[31–35] finetuning of component ratios,[36–38] and development of high-concentrated electrolytes,[39,40] these options are often accompanied by complex preparation processes and expensive costs. For example, Zou et al., developed a fluorinated group-containing carboxylic acid esters-based electrolyte by dissolving $LiPF_6$ salt in a mixture of methyl difluoroacetate, ethoxy-pentafluoro-cyclotriphosphazene, and fluoroethylene carbonate (FEC), achieving remarkable cycling performance and 5 C rate capability of graphite//$LiNi_{0.8}Co_{0.1}Mn_{0.1}O_2$ cells from −50 to 60 °C. However, the solvents are uncommon and expensive, and the electrolyte preparation process is laborious.[31]

Herein, we introduce a comprehensive modification approach involving carbon nanotube (CNT)-based electrodes and a "constructive alliance" electrolyte strategy, ultimately achieving a high-performance LIB functionality from −40 to 60 °C. The LTO, noted for its safety, stability, and marketability,[41,42] serves as the active material, while a "binder-free" 3D CNT current collector forms the electrode skeleton. This combination achieves rapid

electrochemical kinetics at low temperatures and exhibits outstanding thermal regulation at elevated temperatures. In addition, the "constructive alliance" electrolyte with a simple combination of carbonate-based and ether-based electrolytes possesses a dominant aggregate solvation structure independent of temperature, as revealed by molecular dynamics (MD) simulations and density functional theory (DFT) calculations. It also displays low desolvation energies, rapid kinetics, and excellent thermal and electrochemical stability. Benefiting from the integrated optimization of electrodes and electrolytes, both LTO//Li and $LiCoO_2$ (LCO)//Li half cells showcased resilience to extreme temperatures. Notably, the LTO//Li coin cell achieved a high rate of 10 C and maintained stable cycling over 100 cycles at −40 and 60 °C. The assembled LTO//LCO full cell with a negative/positive electrode material ratio of 1.2 can operate even in a bent state from −40 to 60 °C.

2. Results and Discussion

2.1. Preparation and Characterization of CNT-Based Electrodes

Nano-sized $Li_4Ti_5O_{12}$-600 (LTO-600) was synthesized via the sol-gel method and calcination at an optimized temperature of 600 °C (Figures S2 and S3, Supporting Information). It manifested high crystallinity (Figure S4, Supporting Information), a smaller particle size (Figure S5, Supporting Information, nanocluster vs 200–500 nm), and a larger specific surface area (Figure S6, Supporting Information, 16.45 vs 5.13 $m^2\ g^{-1}$) compared to commercial LTO. Afterward, LTO-600 and super-aligned carbon nanotubes (SACNTs) were ultrasonically dispersed and vacuum-filtered to fabricate a self-supporting LTO-600/CNT electrode (refer to Figures S7 and S8, Supporting Information, for the detailed fabrication process, and Figure S9, Supporting Information, for the morphology). A traditional conventional slurry-based electrode was also crafted (Figure S10, Supporting Information).

CNT-based electrodes and slurry-based electrodes respond differently to temperature variations. Their electrical properties at low temperatures were tested using coin cells assembled with lithium sheets. From the slopes of voltammetric characteristic curves (Figure S11, Supporting Information), the resistance values of electrodes could be determined (**Figure 2a**). At −40 and 25 °C, the slurry-based electrode exhibited resistances of 1.76 and 1.40 Ω, respectively, while the CNT-based electrode demonstrated lower resistances of 1.06 and 0.80 Ω at the corresponding temperatures. Second, the charge transfer resistances R_{ct} of both electrodes were measured (Figure 2b; Figure S12, Supporting Information). The R_{ct} values for the slurry-based electrode at 20, 0, −20, and −40 °C were 0.48, 2.03, 6.79, and 84.39 kΩ, while the CNT-based electrode demonstrated smaller R_{ct} of 0.13, 0.66, 4.12, and 36.80 kΩ, respectively. These data highlight the enhanced electron conduction and transfer capabilities of CNT-based electrodes under a cryogenic environment. This is attributed to the construction of a 3D current collector by CNTs, which eliminates non-conductive binders and enables efficient electron transport.

Apart from different electrical properties at low temperatures, the two types of electrodes also have different heat dissipation efficiencies and structural stabilities at high temperatures. Firstly, a visualized platform was devised to assess the heat dissipation of electrodes. Both slurry-based and CNT-based films were subjected to laser exposure at their center, and the temperature variations were captured using an infrared imaging device (Figure 2c,d, Videos S1 and S2, Supporting Information). The temperature at the laser irradiation point gradually increased and heat transfer radiates outward until the sample reached thermal equilibrium. Surface temperature distributions and line temperatures along the diameter at intervals of 1, 5, 10, 20, and 60 s are shown in Figure 2c–e. The CNT-based film experienced a more moderated temperature increase at the laser-irradiated point and a lower final equilibrium temperature (48.0 °C) compared to the slurry-based film (59.4 °C). Such an observation underscores the exceptional heat dissipation capability inherent to the CNT-based film, which greatly mitigates potential hazards associated with heat concentration. To investigate the impact of high temperatures in practical operation, the two electrodes were cycled five times at 60 °C with a commercial electrolyte (1 M $LiPF_6$ in EC: DMC: EMC = 1:1:1 (vol.%)), after which they were disassembled for observation. The slurry-based electrode exhibited numerous cracks after cycling (Figure S13a,b, Supporting Information), while the CNT-based electrode retained its structural integrity (Figure S13c,d, Supporting Information). Based on the comprehensive characterization, the CNT-based electrode outperforms the slurry-based electrode, demonstrating faster electrode kinetics at low temperatures, as well as better thermal dissipation and stability at high temperatures. This validation aligns with the hypothesis, suggesting the potential of CNT-based electrodes to perform admirably at wide temperatures. However, despite utilizing optimized LTO-600 as the active material, the LTO-600/CNT electrode fails to deliver satisfactory electrochemical performance with a commercial electrolyte (Figure S14, Supporting Information). The undesired results at extreme temperatures highlight the impending necessity for advancements in electrolyte formulation.[43,44]

2.2. "Constructive Alliance" Electrolyte Strategy

The "constructive alliance" strategy is aimed at blending readily available electrolytes to efficiently enhance their adaptability across a broad temperature spectrum. Considering the widespread use of the commercial electrolyte (1 M $LiPF_6$ in EC:DMC:EMC = 1:1:1 (vol.%)), it is incorporated as a foundational component in this strategy. To identify other suitable electrolytes, the first step is solvent screening, taking into account the intrinsic characteristics of the solvents and their interactions with Li^+. The physical properties of commonly used solvents are shown in Table S1 (Supporting Information). Representative carbonate solvents manifest high freezing points, while both ester and ether solvents present low freezing points and reduced viscosities. When employed in LIBs, weak interactions between the solvent and Li^+ can facilitate the desolvation process and improve battery performance under extreme temperature conditions.[30] The intricate interaction between the solvent and Li^+ can be quantitatively evaluated via the following key parameters: differential scanning calorimeterthe electrostatic potential (ESP) of the solvent, the binding energy (E_b), and the coordination bond length of the [Li^+-solvent] coordination structure. Calculations of the above properties for commonly used solvents were carried out by Gaussian 09 (Figures S15–S17 and Table S2, Supporting

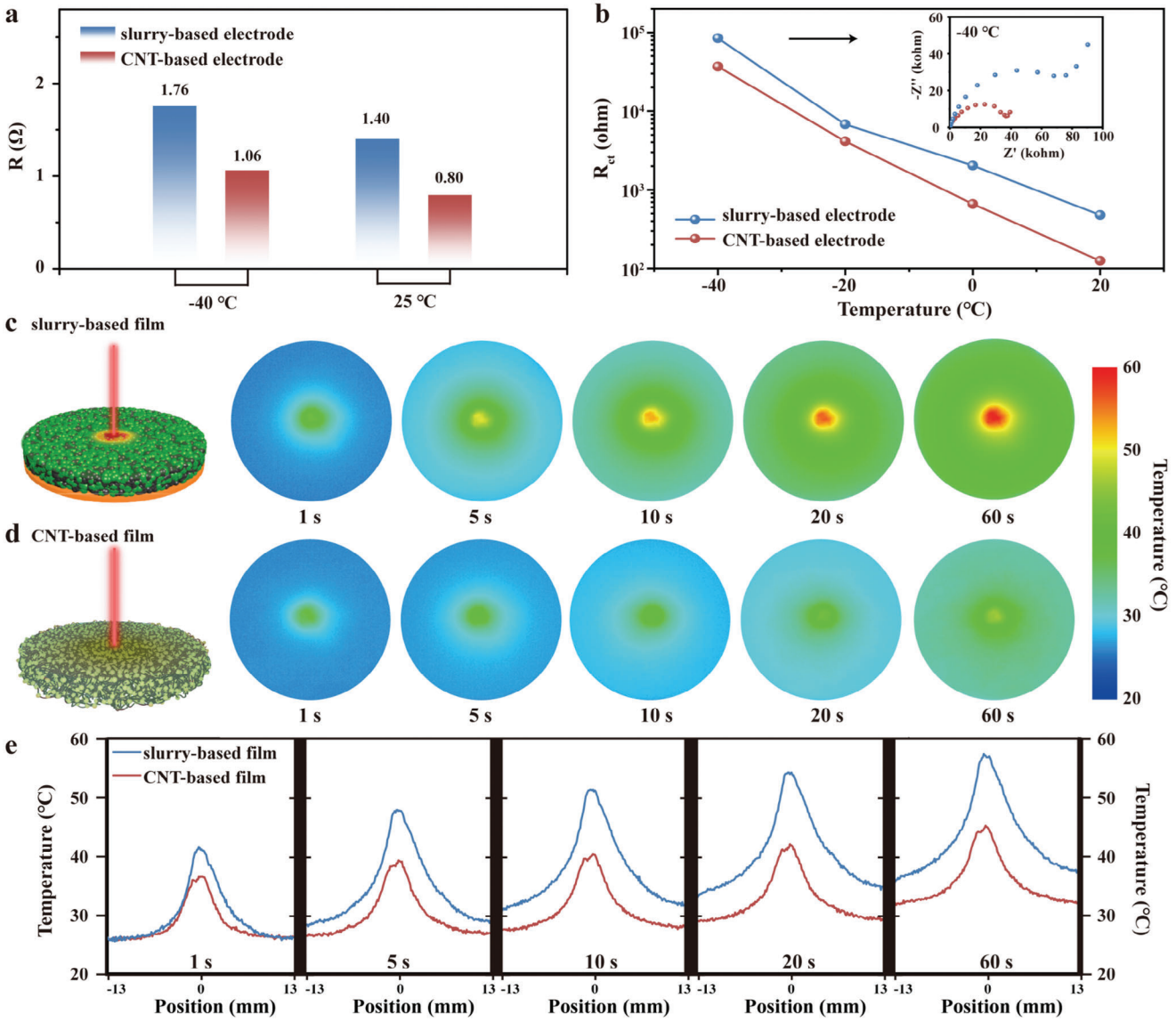

Figure 2. a) Resistances of the slurry-based and CNT-based electrodes at −40 and 25 °C. b) Charge transfer resistance R_{ct} of the slurry-based and CNT-based electrodes in the commercial electrolytes from −40 to 20 °C. Schematics of laser irradiation and surface temperature distribution of the c) slurry-based and d) CNT-based films. e) Line temperature distribution along the diameter of the slurry-based and CNT-based films.

Information). Since molecules tend to approach each other with complementary ESP, the solvent is most easily coordinated to Li^+ at the minimum ESP on the surface.[45] Intriguingly, ether solvents generally exhibited large ESPs, binding energies, and Li-O distances, signifying a moderated affinity toward Li^+. Within this type, the DOL solvent emerged as the exemplar. Its minimum ESP surpassed that of other solvents (Figure S15a, Supporting Information), and both its binding energy (−1.713 eV) and Li-O distance (1.806 Å) were the largest among various [Li^+-solvent] coordination structures (Figure S15b, Supporting Information). Therefore, the addition of DOL solvent to the commercial electrolyte is expected to broaden the operating temperature range of the electrolyte.

Following that, the focus shifted to choosing a suitable lithium salt. The $LiPF_6$ in the commercial electrolyte presents chemical and thermodynamic defects, leading to easy decomposition under elevated temperatures.[46] To break through this limitation, blending $LiPF_6$ with thermally stable lithium salts has proven effective.[47–49] Lithium salts such as LiBOB, LiDFOB, and LiTFSI stand out for their thermal resilience. However, the solubility of LiBOB and LiDFOB in carbonate solvents is a challenge. The differential scanning calorimeter curves of $LiPF_6$ and LiTFSI were measured under an inert atmosphere (Figure S18, Supporting Information). The former commenced decomposition ≈68 °C,[50] while LiTFSI remained stable even at 150 °C, making it a promising choice for enhancing the thermal stability of electrolytes. An electrolyte formulation comprising 0.75 M LiTFSI in DOL solvent (referred to as DOL-based electrolyte) has demonstrated good performance in various electrode systems,[3,51,52] establishing itself as a readily available electrolyte. Therefore, both the commercial

electrolyte and DOL-based electrolyte are chosen as components in the "constructive alliance" strategy. The next step was to optimize the mixing ratio of two electrolytes, which was determined from the electrochemical behavior of the LTO-600/CNT electrode over a broad temperature spectrum (Figures S19 and S20, Supporting Information).

At −40 °C (Figure S19, Supporting Information), when the commercial electrolyte predominated (including commercial electrolyte, and DOL-based:commercial = 1:49, 1:19, 1:9, 1:5 (vol.%)), the LTO-600/CNT electrode exhibited negligible capacity at 0.5 C. When the mixing ratio was 1:2 and 1:1 (vol.%), the LTO-600/CNT electrode had improved performance, however, it failed at 2 and 5 C rates, respectively. By increasing the proportion of the DOL-based electrolyte, the DOL-based:commercial ratios became 2:1, 5:1, 9:1, 19:1, and 49:1 (vol.%). Among them, the electrolyte with a 19:1 ratio achieved the best performance for the LTO-600/CNT electrode, and this held true at both 25 and 60 °C (Figure S20, Supporting Information). As a result, the mixing ratio of DOL-based:commercial electrolyte was determined as 19:1 (vol.%), hereafter referred to as the "mix electrolyte". According to optical images and ^{1}H nuclear magnetic resonance spectroscopy, the "mix electrolyte" did not undergo significant ring-opening polymerization of DOL and remained in a liquid state (Figures S21 and S22, Supporting Information). Furthermore, it should be noted that although a pure DOL-based electrolyte exhibited weak interaction with Li^+ and favorable thermal stability, it failed to withstand high current densities at −40 °C (Figure S19b, Supporting Information). The "abnormal overcharging" phenomenon might stem from the redox reactions of $TFSI^-$ anions and could be mitigated by the commercial electrolyte.[53–55]

2.2.1. Microscopic Mechanism of the Electrolyte

To understand the mechanism of the improved performance observed in the mixed electrolyte, MD simulations were conducted across diverse thermal conditions (refer to Table S3, Supporting Information, for modeling parameters). Equilibrated snapshots of both electrolytes at −40, 25, and 60 °C were shown in Figure S23 (Supporting Information). The radial distribution functions (RDFs) and coordination numbers (CNs) of Li^+ with O and F atoms were examined with a cutoff distance of 2.5 Å. At room temperature, the commercial electrolyte exhibited CNs of Li^+-O and Li^+-F at 3.53 and 1.60, respectively (Figure S24b, Supporting Information). The Li^+-O coordination involved the participation of EC, DMC, and EMC solvents, with EC being the dominant contributor (Figure S24e, Supporting Information). In the mixed electrolyte, Li^+ primarily coordinated with O atoms, resulting in CNs of 4.95 for Li^+-O and 0.19 for Li^+-F (Figure S25b, Supporting Information), where DOL and $TFSI^-$ replaced EC as the main source of Li^+-O coordination (Figure S25e, Supporting Information). Taking the results at −40 and 60 °C into account, a trend was noted: with escalating temperatures, the CNs of Li^+-O gradually decreased for both electrolytes (**Figure 3a**), while the compositional proportion of Li^+-O remained almost the same. The CNs of Li^+-F were basically unchanged (Figure 3b), with corresponding RDFs delineated in Figures S24 and S25 (Supporting Information).

The investigation then delves into the molecular realm, exploring the typical solvation structures of Li^+. For the commercial electrolyte, the representative solvation structures displayed desolvation energies of −0.261, −0.267, and −0.284 Hartree (Figure 3d). Notably, the characteristic solvation structures of the mixed electrolyte possessed desolvation energies of −0.186, −0.200, and −0.205 Hartree (Figure 3e). The mix electrolyte exhibited weaker solvating power, indicating easier extraction of Li^+, which was advantageous for low-temperature and high-rate operations.[56]

To comprehensively understand the Li^+ transport behavior of both electrolytes, statistical analysis was performed on the coordination patterns (Figure 3c).[57] Based on the ratio of the Li^+ and anion, the coordination structures can be categorized into solvent-separated ion pair (SSIP, free ion), contact-ion pair (CIP, one ion coordinating with one counterion), and aggregate (AGG, one ion coordinating with more than one counterion).[57,58] Generally, SSIP structures are known for their inferior performance at low temperatures,[59] while CIP and AGG structures facilitate rapid desolvation and fast migration of Li^+.[57,60] Compared to the commercial electrolyte, the mixed electrolyte had a reduced presence of SSIP structures and an increased occurrence of AGG structures across wide temperatures (Figure 3c; Figure S26 and Table S4, Supporting Information), which aligned with the characteristics of weakly solvated electrolytes.[61] Integrating analyses from atomic, molecular, and statistical levels, the electrolyte obtained by the "constructive alliance" strategy exhibits a dominant presence of AGG-solvated structures that are advantageous for Li^+ desolvation and nearly unaffected by temperature variations between −40 and 60 °C.

2.2.2. Macroscopic Properties of the Electrolyte

Shifting to the experimental perspective, the kinetic properties and electrochemical stability of both electrolytes were evaluated across a wide temperature range. The ionic conductivities of electrolytes were measured within a temperature range of ± 60 °C (**Figure 4a**). At temperatures above 0 °C, the mixed electrolyte exhibited slightly lower ionic conductivity compared to the commercial electrolyte. However, as the temperature decreased, the mixed electrolyte showed better retention of ion conductivity. At −60 °C, the ion conductivities of the commercial and mixed electrolytes were 0.0043 and 0.0995 mS cm^{-1}, respectively, corresponding to conductivity retentions of 0.4% and 21.3% compared to the values at 60 °C. To exclusively evaluate the transport efficiency of Li^+, the Li-ion transference number was tested.[62] For the commercial electrolyte, the Li-ion transference numbers at 0, 25, and 60 °C were 0.42, 0.43, and 0.61, respectively. For the mixed electrolyte, these values were 0.63, 0.65, and 0.71 at the same temperatures (Figure 4b,c; Figure S27, Supporting Information). The high Li-ion transference number of the mixed electrolyte could be attributed to the predominance of AGG solvation structures, which engage many anions in coordination with lithium ions, thereby reducing the quantity of freely mobile anions.[63]

In addition to comparing the Li^+ transport within the electrolyte, it is also necessary to investigate the interfacial interactions between the electrolyte and the electrode. Firstly, we studied the interfacial charge transfer and ion transport rates

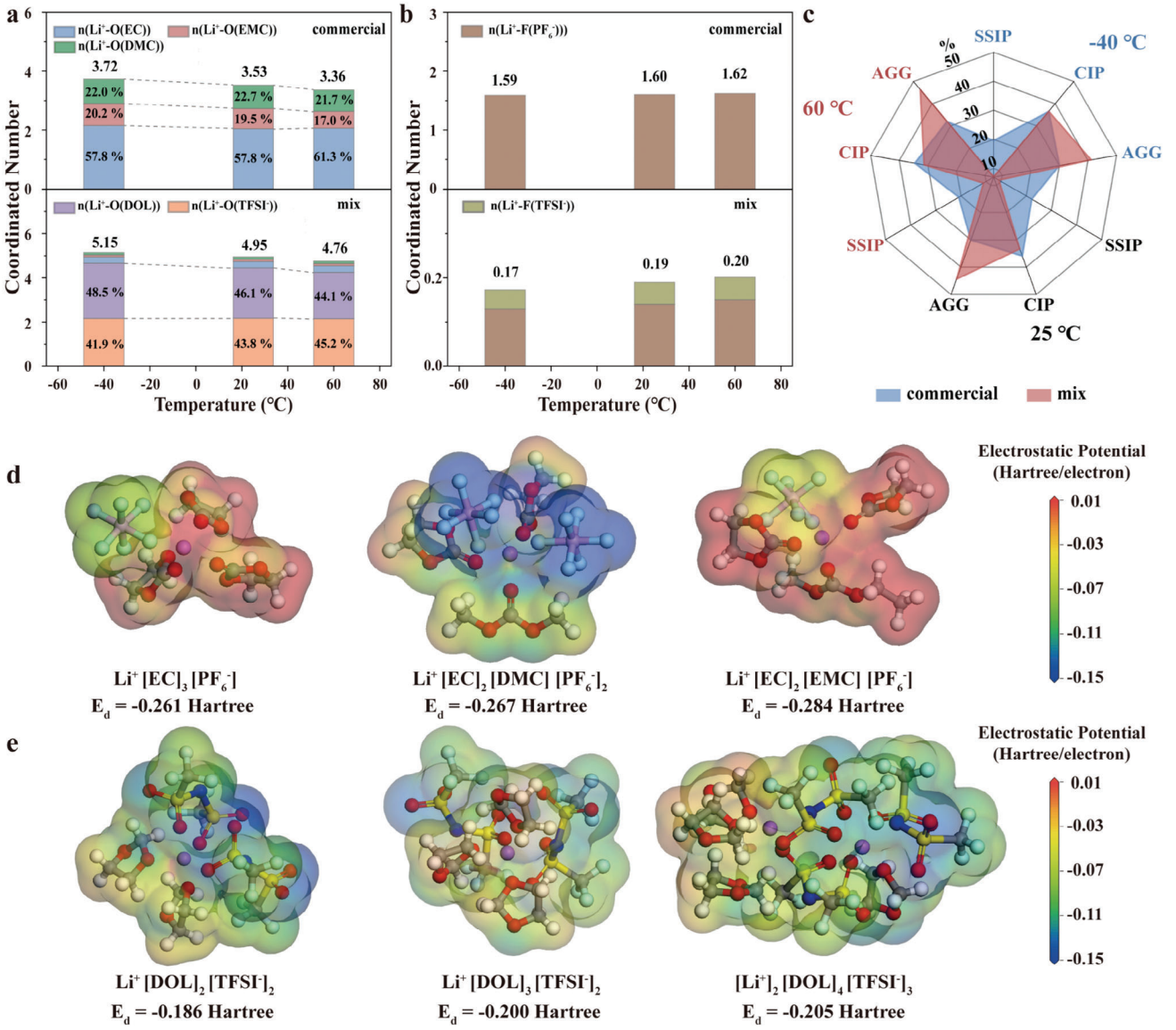

Figure 3. a) CNs of Li^+ with O atom and b) F atom in different species in commercial electrolyte and mixed electrolyte. c) The proportion of solvation structure types in the commercial and mixed electrolytes at −40, 25, and 60 °C. ESP mapping and desolvation energy E_d of representative solvation structures in the d) commercial and e) mix electrolyte. The H, Li, C, N, O, F, and S atoms are marked in white, purple, gray, blue, red, cyan, and yellow, respectively.

between the electrolyte and the LTO-600/CNT electrode. In the temperature range of −40–60 °C, the interfacial charge transfer resistances R_{ct} of the LTO-600/CNT electrode were smaller when using the mixed electrolyte compared to the commercial electrolyte (Figure 4d). The electrochemical impedance spectroscopy (EIS) curves at −40 °C are illustrated in Figure 4e as an example. For the commercial and mixed electrolytes, the R_{ct} of the LTO-600/CNT electrode was 36.8 and 5.1 kΩ, respectively. On the other hand, the activation energy of the interfacial Li^+ transfer was analyzed by the Arrhenius equation (Figure 4f; refer to Figure S28 and Table S5, Supporting Information for specific data and calculation details). In the mixed electrolyte, the activation energy E_a was 0.71 eV, which was lower than the 0.92 eV observed in the commercial electrolyte. This underscores a rapid Li^+ transport at the interface between the mixed electrolyte and electrodes.[62] Subsequent investigations focused on the challenges faced by lithium metal electrodes at 60 °C (Figure S29, Supporting Information). With the commercial electrolyte, the lithium metal surface was rough and porous after 50 cycles, reflecting the poor lithium deposition/stripping behavior of $LiPF_6$ and carbonate solvents.[64,65] Conversely, when the mixed electrolyte was used, the lithium metal surface was homogeneous with dough-like deposition after 50 cycles. This indicates that the mixed electrolyte enables fast interfacial electron and ion transfer, achieving excellent reversibility of lithium metal. A smooth lithium metal surface not only mitigates the severe safety risks posed by dendritic but also minimizes the contact area with the electrolyte, which is beneficial in reducing

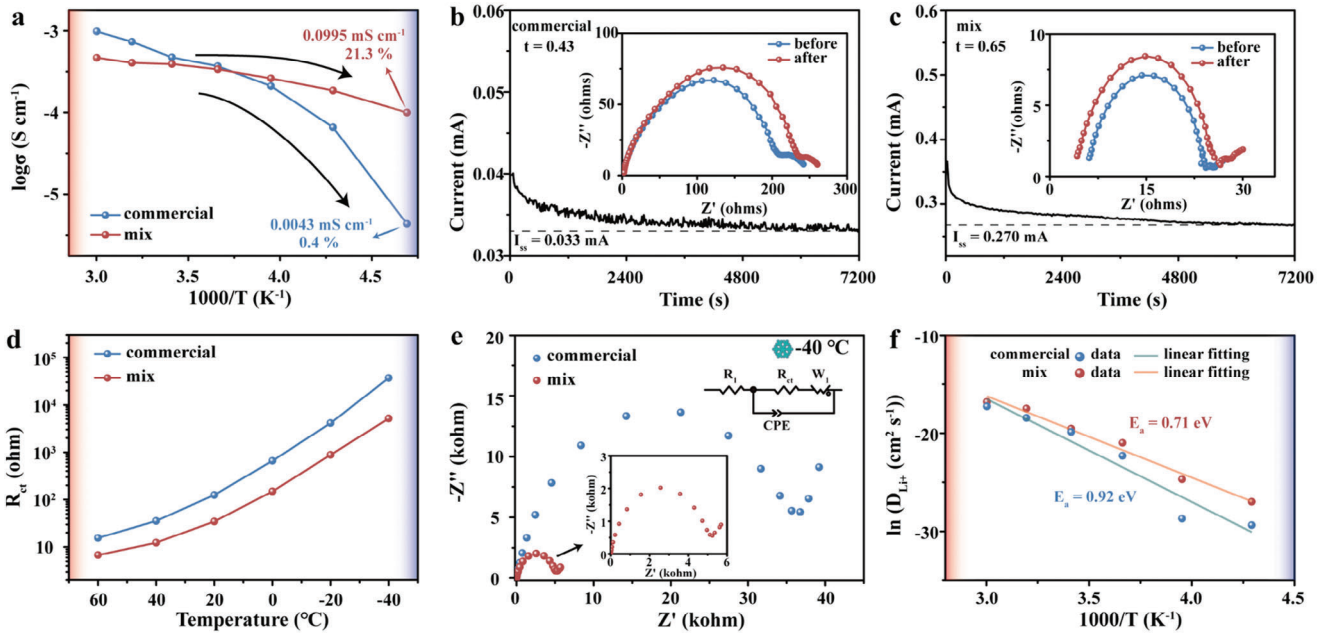

Figure 4. a) Ionic conductivity of the commercial and mixed electrolyte from 60 °C to −60 °C. EIS and current profiles of a Li//Li symmetric cell before and after applying a polarization voltage with b) commercial electrolyte and c) mixed electrolyte. d) Charge transfer resistance R_{ct} of the LTO-600/CNT electrode in the commercial and mix electrolytes from 60 °C to −40 °C. e) EIS measurements of the LTO-600/CNT electrodes in the commercial and mixed electrolyte at −40 °C. f) The linear relationship between ln (D_{Li}^+) and $10^3/T$ at different temperatures.

side reactions and extending the cycle life of the battery at high temperatures.

Beyond its accelerated kinetics, the mixed electrolyte also provided better electrochemical stability than the commercial electrolyte (Figure S30, Supporting Information). At 25, −40, and 60 °C, the electrochemical windows of the mixed electrolyte were 3.42, 4.67, and 3.06 V, respectively, whereas the corresponding electrochemical windows of the commercial electrolyte were only 2.90, 4.57, and 2.23 V. Multiple experimental characterizations collectively demonstrate that the mixed electrolyte surpassed the commercial electrolyte in various aspects, including ionic conductivity, Li-ion transference number, electrode impedance, activation energy, and electrochemical window. Combining the mixed electrolyte with the optimized LTO-600/CNT electrode holds the potential to achieve excellent electrochemical performance across a wide temperature range.

2.3. Electrochemical Performance of Half Cells Over a Wide Temperature Range

Using LTO-600/CNT and lithium sheet as electrodes, the rate performance of the LTO//Li coin cell was analyzed to compare the commercial and mixed electrolytes (**Figure** 5a–c), and the corresponding voltage profiles were shown in Figure S31 (Supporting Information). At 25 °C, when the rate increased from 0.05 to 10 C, the specific capacity retentions of cells assembled with the commercial and mixed electrolyte were 92.6% (125.3 mAh g^{-1}/135.3 mAh g^{-1}) and 95.7% (142.8 mAh g^{-1}/149.2 mAh g^{-1}), respectively (Figure 5a). At −40 °C, when using the commercial electrolyte, the LTO-600/CNT electrode experienced high polarization (≈0.80 V) at 0.05 C (Figure S29b, Supporting Information). Escalating the rate to 0.5 C precipitated a near-zero capacity (Figure 5b). Conversely, within the mixed electrolyte, the LTO-600/CNT electrode demonstrated specific capacities of 146.9, 127.6, 118.0, 114.7, 105.6, 96.9, 79.3, and 60.6 mAh g^{-1} at 0.05, 0.1, 0.2, 0.5, 1, 2, 5, and 10 C, respectively. Upon changing the rate back to 0.1 C, the specific capacity recovered to 127.9 mAh g^{-1}. Furthermore, the polarization of the LTO-600/CNT electrode within the range of 0.05–2 C was significantly reduced (< 0.4 V), with polarization increasing to merely 0.56 and 0.76 V at 5 C and 10 C, respectively (Figure S31e, Supporting Information). The commercial electrolyte suffered from diminished conductivity, sluggish ion transport, and laborious Li^+ desolvation at low temperatures. These factors contributed to disparities in electrolyte concentration at the interface and in the bulk phase, resulting in significant concentration polarization. At 60 °C (Figure 5c), the LTO-600/CNT electrode exhibited initial coulombic efficiencies of 54.8% and 89.1% for the commercial and mixed electrolytes, respectively. This revealed that the mixed electrolyte delivered better stability and fewer side reactions at high temperatures. With the commercial electrolyte, the LTO-600/CNT electrode experienced extreme capacity decay and a sharp increase in electrode polarization after 5 C (Figure S31c, Supporting Information). In contrast, with the mixed electrolyte, the LTO/CNT-600 electrode performed a high capacity retention (89.8%, 140.8 mAh g^{-1}/156.8 mAh g^{-1}) and small polarization (<0.2 V, Figure S29f, Supporting Information) at rates from 0.05 to 10 C. Furthermore, the LTO-600/CNT electrode also demonstrated better electrochemical properties compared to the slurry-based electrode at 25, −40, and 60 °C (Figure S32, Supporting Information), highlighting the exceptional functionality of CNT-based electrodes in different thermal conditions.

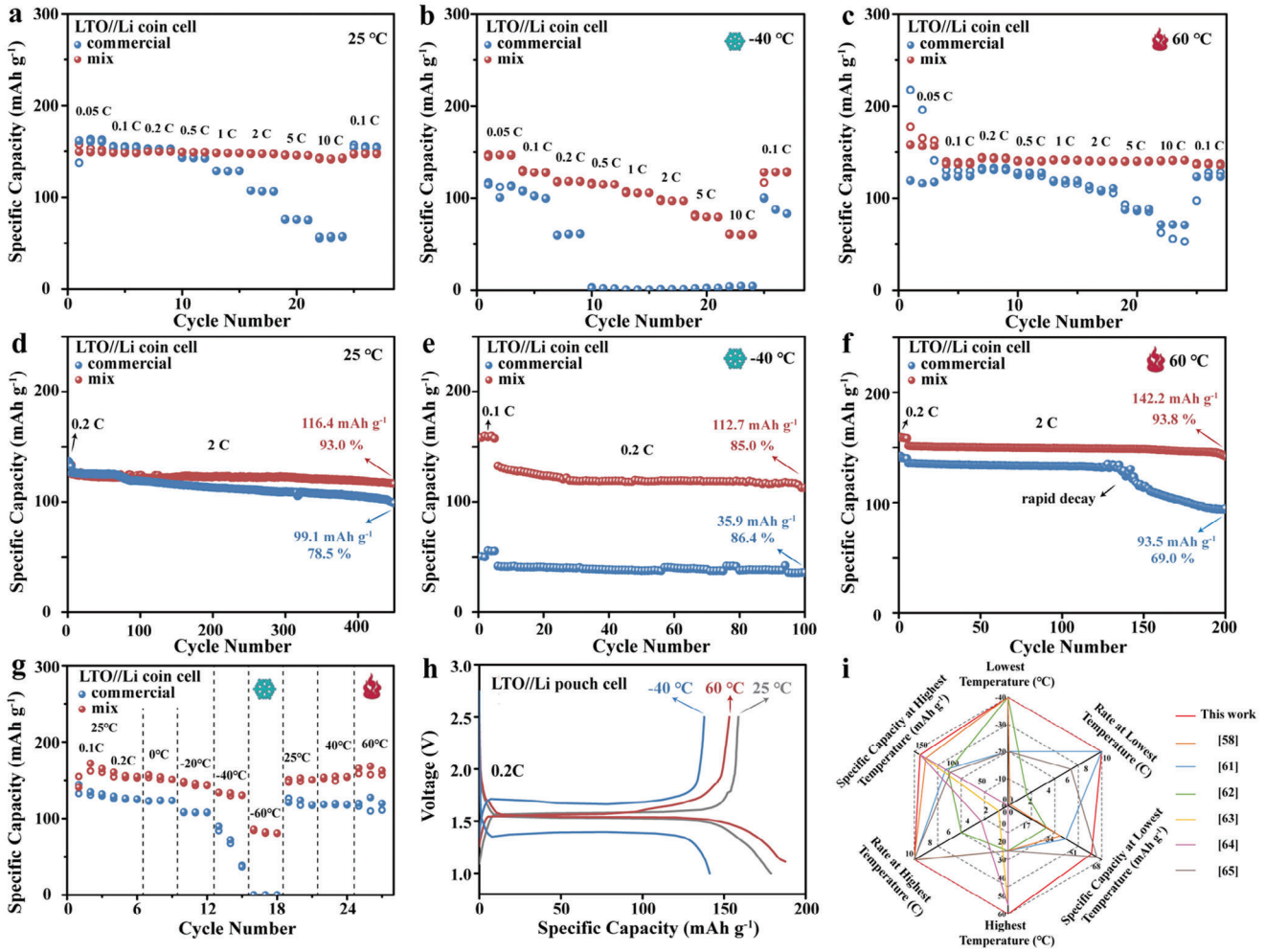

Figure 5. Rate performances of the LTO-600/CNT electrodes with commercial and mixed electrolytes at a) 25 °C, b) −40 °C, and c) 60 °C. Cycling performances of the LTO-600/CNT electrodes with commercial and mixed electrolytes at d) 25 °C, e) −40 °C, and f) 60 °C. g) Cycling performance of the LTO-600/CNT electrodes with commercial and mixed electrolytes in a wide temperature range (0.2 C). (hollow symbol: discharge specific capacity, solid symbol: charge specific capacity) h) Voltage profiles of the LTO//Li pouch cell with mixed electrolytes at 25, −40, and 60 °C. i) Comparison with data in the literature.

The cycling performance of LTO//Li coin cells was then evaluated to compare the durability of the two electrolytes. After five activated cycles at low rates, the cells underwent long-term cycling at a fixed rate. With the mixed electrolyte, the LTO-600/CNT electrode performed stably at 2 C for 445 cycles at 25 °C, with a capacity retention rate of 93% (Figure 5d). At −40 °C, the LTO-600/CNT electrode retained 85.0% of its capacity after 95 cycles at 0.2 C (112.7 mAh g^{-1}/132.6 mAh g^{-1}, Figure 5e). Moreover, at 60 °C, the LTO-600/CNT electrode exhibited an impressive capacity retention rate of 93.7% after 195 cycles at 2 C (142.1 mAh g^{-1}/151.6 mAh g^{-1}, Figure 5f). On the contrary, when using the commercial electrolyte, the LTO-600/CNT electrode showed inadequate capacity retention at 25 °C (78.5%), reduced capacity at −40 °C, and deteriorated performance at 60 °C. The performance disparity induced by these two electrolytes became more pronounced during cycling at a higher rate of 10 C (Figure S33, Supporting Information). The limited performance with the commercial electrolyte is due to the slow kinetics processes and poor thermal stability.

Varying the environmental temperature within a range of ±60 °C, a comparison was carried out between the two electrolytes (Figure 5g). The cells initially underwent three charge–discharge cycles at 25 °C under a 0.1 C rate, followed by continuous cycling at sequential temperature gradients under a 0.2 C rate. Leveraging the mixed electrolyte, the LTO-600/CNT electrode achieved capacities of 153.0, 151.1, 144.1, 130.4, 80.5, 150.4, 153.0, and 157.2 mAh g^{-1} at temperatures of 25, 0, −20, −40, −60, 25, 40, and 60 °C, respectively. Conversely, with the commercial electrolyte, the capacity of the LTO-600/CNT electrode significantly decreased at −40 °C and was almost completely lost at −60 °C.

On a larger scale, an LTO//Li pouch cell was further assembled to evaluate the performance of the LTO-600/CNT electrode and mix electrolyte (Figure 5h). Its discharge and charge capacities at 25 °C were 174.7 and 158.7 mAh g^{-1}, respectively. At −40 °C, the discharge capacity retention was 80.8% (141.2 mAh g^{-1}/174.7 mAh g^{-1}), and the charge capacity retention turned out to be

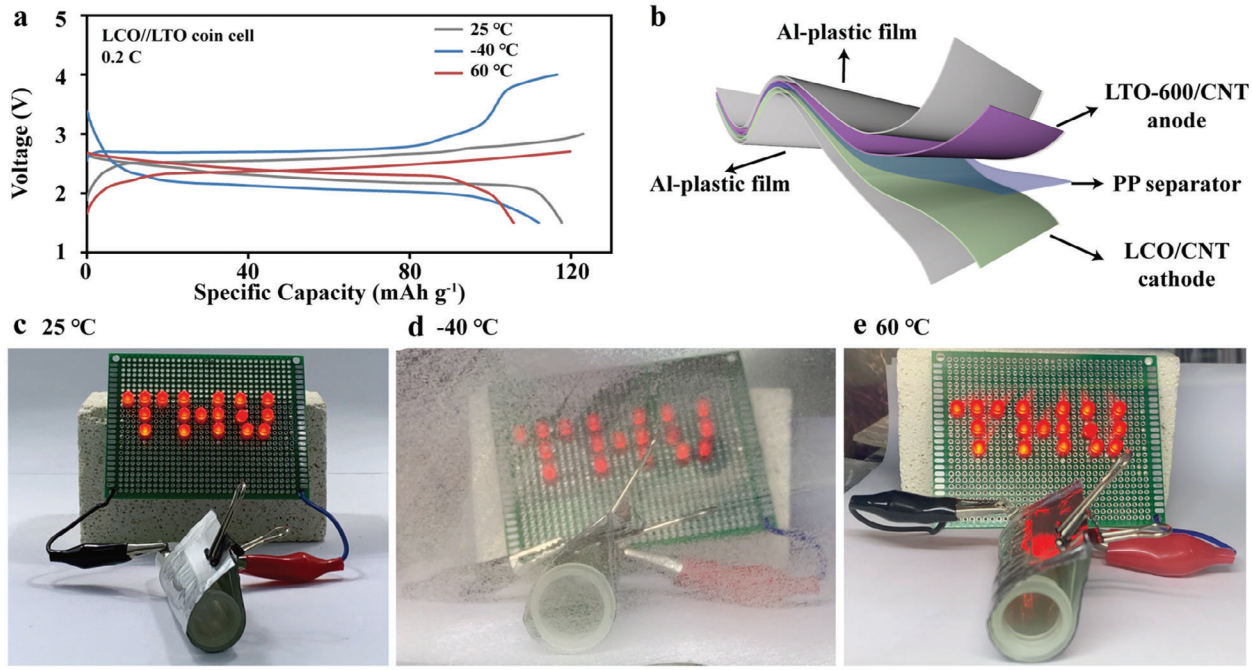

Figure 6. a) Voltage profiles of the LTO//LCO coin cell at 25, −40, and 60 °C (0.2 C). b) Schematic of the structure of a flexible LTO//LCO pouch cell. Photographs of the lit LED array using a flexible LTO//LCO pouch cell at c) 25 °C, d) −40 °C, and e) 60 °C.

86.8% (137.8 mAh g^{-1}/158.7 mAh g^{-1}). Raising the temperature to 60 °C, the discharge capacity of the LTO//Li pouch cell notably increased to 187.5 mAh g^{-1}, while the charge capacity reached 153.2 mAh g^{-1}. In comparison with data in the literature, the combination of the LTO-600/CNT electrode and mix electrolyte showed exceptional performance across various aspects, encompassing a wide temperature range, impressive rate capability, and high capacity (Figure 5i),[62,66–70] as detailed in Table S6 (Supporting Information). The outstanding electrochemical performance stems from the optimized active material, electrode structure, and electrolyte formulation. In detail, nano-sized LTO-600 particles facilitate efficient and rapid transport of Li^+. Interwoven CNT network guarantees optimal electron transfer and thermal management. Additionally, the mixed electrolyte showcases favorable kinetic and thermal stability, providing a stable and conducive environment for the electrochemical reactions.

The LCO/CNT cathode was then fabricated by combining LCO and SACNTs, followed by assembly with a lithium sheet to construct LCO//Li coin cells and pouch cells. The LCO/CNT cathode boasted capacities surpassing 100 mAh g^{-1} at 0.5 C and 85 mAh g^{-1} at 1 C, spanning from −40 to 60 °C (Figure S34a,b and Table S7, Supporting Information). Furthermore, the LCO//Li pouch cell demonstrated favorable performance across an extensive temperature range (Figure S34c, Supporting Information), with discharge specific capacities of 133.2, 125.1, and 65.7 mAh g^{-1} at 25, −40, and 60 °C, respectively.

2.4. Electrochemical Performance of Full Cells Over a Wide Temperature Range

Considering practical applications, LTO//LCO coin cells and pouch cells were assembled with a negative/positive ratio of 1.2. At 0.2 C, the LCO//LTO coin cell exhibited 117.7, 111.9, and 105.7 mAh g^{-1} at 25, −40, and 60 °C, respectively (**Figure 6a**). Afterward, the LTO//LCO pouch cell was prepared using the LTO-600/CNT electrode, PP separator, LCO/CNT cathode, and aluminum-plastic film (Figure 6b; Figure S35, Supporting Information). At 25, −40, and 60 °C, the discharge-specific capacities of the LTO//LCO pouch cell were 123.0, 97.5, and 47.7 mAh g^{-1}, respectively (Figure S36, Supporting Information). The resilience of CNT-based electrodes, which could withstand up to 10 000 bending cycles (Figures S37–S39, Supporting Information), allowed for significant flexibility of the pouch cell. After 1000 cycles of bending at 180°, the LTO//LCO pouch cell showed no breakage or leakage (Figure S40, Supporting Information), with an impressive capacity retention of 90.8% (6.66 mAh/7.33 mAh, Figure S41, Supporting Information). When rolled into a cylindrical shape, the pouch cell successfully illuminated the LED arrays at 25, −40, and 60 °C (Figure 6c–e).

3. Conclusion

In conclusion, we have developed a wide temperature range operation LIB system by fabricating CNT-based electrodes and implementing a "constructive alliance" electrolyte. Compared to the conventional slurry-based electrode, the CNT-based electrode exhibits rapid kinetics at low temperatures and exceptional thermal management at high temperatures. Simultaneously, the "constructive alliance" electrolyte system ensures the ionic conductivity at low temperatures and stability of the $LiPF_6$ at elevated temperatures. As a result, the assembled LCO//LTO full cell exhibits excellent electrochemical performance over a wide temperature range from −40 to 60 °C. Our designed strategy provides valuable

insights and a promising avenue for developing energy storage devices under extreme temperatures.

Supporting Information

Supporting Information is available from the Wiley Online Library or from the author.

Acknowledgements

This work was supported by the National Basic Research Program of China (2019YFA0705702) and the National Natural Science Foundation of China (51872158).

Conflict of Interest

The authors declare no conflict of interest.

Data Availability Statement

The data that support the findings of this study are available from the corresponding author upon reasonable request.

Keywords

carbon nanotube, lithium-ion battery, solvation environment, wide temperature

Received: March 5, 2024
Revised: May 31, 2024
Published online: August 9, 2024

[1] J. Neumann, M. Petranikova, M. Meeus, J. D. Gamarra, R. Younesi, M. Winter, S. Nowak, *Adv. Energy Mater.* **2022**, *12*, 2102917.
[2] Z. Zhang, T. Hu, Q. Sun, Y. Chen, Q. Yang, Y. Li, *J. Power Sources* **2020**, *453*, 227908.
[3] J. Xu, X. Wang, N. Yuan, B. Hu, J. Ding, S. Ge, *J. Power Sources* **2019**, *430*, 74.
[4] J. Zhou, H. Ji, Y. Qian, J. Liu, T. Yan, C. Yan, T. Qian, *ACS Appl. Mater. Interfaces* **2021**, *13*, 48810.
[5] J. Wang, M. Yang, J. Wang, D. Liu, G. Zou, B. Liu, J. S. Tse, L. Li, L. Ren, Q. Peng, *Energy Storage Mater.* **2022**, *47*, 611.
[6] C. Lv, C. Lin, X. S. Zhao, *Adv. Energy Mater.* **2022**, *12*, 2102550.
[7] R. Guo, W. Han, *Mater. Today Sustain.* **2022**, *19*, 100187.
[8] E. Markevich, G. Salitra, D. Aurbach, *J. Electrochem. Soc.* **2016**, *163*, A2407.
[9] G. A. Collins, H. Geaney, K. M. Ryan, *J. Mater. Chem. A* **2021**, *9*, 14172.
[10] A. Gupta, A. Manthiram, *Adv. Energy Mater.* **2020**, *10*, 2001972.
[11] J. Hou, M. Yang, D. Wang, J. Zhang, *Adv. Energy Mater.* **2020**, *10*, 1904152.
[12] A. Blyr, C. Sigala, G. Amatucci, D. Guyomard, Y. Chabre, J. M. Tarascon, *J. Electrochem. Soc.* **1998**, *145*, 194.
[13] P. Zhou, Y. Xia, Y. Wu, W. Hou, Y. Lu, S. S. Yan, H. Zhou, W. Zhang, K. Liu, *ACS Appl. Mater. Interfaces* **2022**, *14*, 38921.
[14] L. Guo, D. B. Thornton, M. A. Koronfel, I. E. L. Stephens, M. P. Ryan, *J. Phys. Energy* **2021**, *3*, 032015.
[15] J. Zhang, D. Liu, Q. Han, L. Jiang, H. Shao, B. Tang, W. Lei, T. Lin, C. H. Wang, *Compos. Part B Eng.* **2019**, *175*, 107157.
[16] Y. Lei, Y. Bai, Y. Shi, M. Liang, H. Zou, S. Zhou, *J. Polym. Res.* **2022**, *29*, 213.
[17] N. Lingappan, L. Kong, M. Pecht, *Renew. Sustain. Energy Rev.* **2021**, *147*, 111227.
[18] D. Leanza, C. A. F. Vaz, P. Novák, M. El Kazzi, *Helv. Chim. Acta* **2021**, *104*, 2000183.
[19] P. Rachtanapun, N. Rattanapanone, *J. Appl. Polym. Sci.* **2011**, *122*, 3218.
[20] A. P. Indolia, M. S. Gaur, *J. Therm. Anal. Calorim.* **2013**, *113*, 821.
[21] Q. Wang, P. Ping, X. Zhao, G. Chu, J. Sun, C. Chen, *J. Power Sources* **2012**, *208*, 210.
[22] H. Zhang, Y. Yang, H. Xu, L. Wang, X. Lu, X. He, *InfoMat* **2022**, *4*, e12228.
[23] X. Dong, Y.-G. Wang, Y. Xia, *Acc. Chem. Res.* **2021**, *54*, 3883.
[24] W. Zhang, X. Sun, Y. Tang, H. Xia, Y. Zeng, L. Qiao, Z. Zhu, Z. Lv, Y. Zhang, X. Ge, S. Xi, Z. Wang, Y. Du, X. Chen, *J. Am. Chem. Soc.* **2019**, *141*, 14038.
[25] Y. Chen, Z. Pu, Y. Liu, Y. Shen, S. Liu, D. Liu, Y. Li, *J. Power Sources* **2021**, *515*, 230601.
[26] H. Zhu, M. H. A. Shiraz, L. Liu, Y. Hu, J. Liu, *Nanotechnology* **2021**, *32*, 144001.
[27] Y. Liu, R. Hu, D. Zhang, J. Liu, F. Liu, J. Cui, Z. Lin, J. Wu, M. Zhu, *Adv. Mater.* **2021**, *33*, 2004711.
[28] K. Ryu, M. J. Lee, K. Lee, S. W. Lee, *ENERGY Environ. Mater.* **2023**, *6*, e12662.
[29] M. Liang, L. Li, X. Cui, S. Qi, L. Wang, H. Dong, X. Chen, Y. Wang, S. Chen, G. Wang, *Small* **2022**, *18*, 2202151.
[30] Y. Feng, L. Zhou, H. Ma, Z. Wu, Q. Zhao, H. Li, K. Zhang, J. Chen, *Energy Environ. Sci.* **2022**, *15*, 1711.
[31] Y. Zou, Z. Ma, G. Liu, Q. Li, D. Yin, X. Shi, Z. Cao, Z. Tian, H. Kim, Y. Guo, C. Sun, L. Cavallo, L. Wang, H. N. Alshareef, Y.-K. Sun, J. Ming, *Angew. Chem., Int. Ed.* **2023**, *62*, 202216189.
[32] J. Lu, X. Xu, W. Fan, Y. Xin, W. Wang, C. Fan, P. Cheng, J. Zhao, J. Liu, Y. Huo, *ACS Appl. Energy Mater.* **2022**, *5*, 6324.
[33] T. Zheng, J. Xiong, B. Zhu, X. Shi, Y.-J. Cheng, H. Zhao, Y. Xia, *J. Mater. Chem. A* **2021**, *9*, 9307.
[34] A. Hu, Z. Liao, J. Huang, Y. Zhang, Q. Yang, Z. Zhang, L. Yang, S. Hirano, *Chem. Eng. J.* **2022**, *448*, 137661.
[35] S. Xu, R. Xu, T. Yu, K. Chen, C. Sun, G. Hu, S. Bai, H.-M. Cheng, Z. Sun, F. Li, *Energy Environ. Sci.* **2022**, *15*, 3379.
[36] Y. Wang, H. Zheng, L. Hong, F. Jiang, Y. Liu, X. Feng, R. Zhou, Y. Sun, H. Xiang, *Chem. Eng. J.* **2022**, *445*, 136802.
[37] A. C. Thenuwara, P. P. Shetty, N. Kondekar, S. E. Sandoval, K. Cavallaro, R. May, C.-T. Yang, L. E. Marbella, Y. Qi, M. T. McDowell, *ACS Energy Lett.* **2020**, *5*, 2411.
[38] A. C. Thenuwara, P. P. Shetty, M. T. McDowell, *Nano Lett.* **2019**, *19*, 8664.
[39] J. Wang, Q. Zheng, M. Fang, S. Ko, Y. Yamada, A. Yamada, *Adv. Sci.* **2021**, *8*, 2101646.
[40] M. Zhao, G. Xu, D. Lu, B. Xie, L. Huang, W. Wang, G. Cui, *J. Electrochem. Soc.* **2021**, *168*, 050511.
[41] "Toshiba, SCiB", https://www.global.toshiba/jp/products-solutions/battery/scib.html, (accessed: May 2024).
[42] "GREE ALTAIRNANO NEW ENERGY INC.", http://www.zhyle.com/en/introduction.html, (accessed: May 2024).
[43] L. Chen, H. Wu, X. Ai, Y. Cao, Z. Chen, *Batter. Energy* **2022**, *1*, 20210006.
[44] D. Hubble, D. E. Brown, Y. Zhao, C. Fang, J. Lau, B. D. McCloskey, G. Liu, *Energy Environ. Sci.* **2022**, *15*, 550.
[45] P. Xiao, Y. Zhao, Z. Piao, B. Li, G. Zhou, H.-M. Cheng, *Energy Environ. Sci.* **2022**, *15*, 2435.
[46] S. E. Sloop, J. K. Pugh, S. Wang, J. B. Kerr, K. Kinoshita, *Electrochem. Solid-State Lett.* **2001**, *4*, A42.
[47] G. Xu, X. Shangguan, S. Dong, X. Zhou, G. Cui, *Angew. Chem.* **2020**, *59*, 3400.

[48] E.-S. Hong, S. Okada, T. Sonoda, S. Gopukumar, J. Yamaki, *J. Electrochem. Soc.* **2004**, *151*, A1836.
[49] Y. Huang, S. Liu, Q. Chen, K. Jiao, B. Ding, J. Yan, *Adv. Funct. Mater.* **2022**, *32*, 2201496.
[50] Z. Lu, L. Yang, Y. Guo, *J. Power Sources* **2006**, *156*, 555.
[51] J. Xu, X. Wang, N. Yuan, J. Ding, S. Qin, J. M. Razal, X. Wang, S. Ge, Y. Gogotsi, *Energy Storage Mater.* **2019**, *23*, 383.
[52] B. Hu, X. Zhou, J. Xu, X. Wang, N. Yuan, S. Ge, J. Ding, *ChemElectroChem* **2020**, *7*, 716.
[53] Y. Diao, K. Xie, S. Xiong, X. Hong, *J. Power Sources* **2013**, *235*, 181.
[54] F. Aguesse, W. Manalastas, L. Buannic, J. M. Lopez del Amo, G. Singh, A. Llordés, J. Kilner, *ACS Appl. Mater. Interfaces* **2017**, *9*, 3808.
[55] C. Y. Kim, G. H. Lee, H. A. So, K. H. Shin, Y. J. Lee, *ACS Appl. Mater. Interfaces* **2020**, *12*, 49541.
[56] T. Ma, Y. Ni, Q. Wang, W. Zhang, S. Jin, S. Zheng, X. Yang, Y. Hou, Z. Tao, J. Chen, *Angew. Chem., Int. Ed.* **2022**, *61*, 202207927.
[57] C.-B. Jin, N. Yao, Y. Xiao, J. Xie, Z. Li, X. Chen, B.-Q. Li, X.-Q. Zhang, J.-Q. Huang, Q. Zhang, *Adv. Mater.* **2023**, *35*, 2208340.
[58] Z. Yu, N. P. Balsara, O. Borodin, A. A. Gewirth, N. T. Hahn, E. J. Maginn, K. A. Persson, V. Srinivasan, M. F. Toney, K. Xu, K. R. Zavadil, L. A. Curtiss, L. Cheng, *ACS Energy Lett.* **2022**, *7*, 461.
[59] J. Holoubek, K. Kim, Y. Yin, Z. Wu, H. Liu, M. Li, A. Chen, H. Gao, G. Cai, T. A. Pascal, P. Liu, Z. Chen, *Energy Environ. Sci.* **2022**, *15*, 1647.
[60] X. Deng, S. Zhang, C. Chen, Q. Lan, G. Yang, T. Feng, H. Zhou, H. Wang, Z. Xu, M. Wu, *Electrochim. Acta* **2022**, *415*, 140268.
[61] Y.-X. Yao, X. Chen, C. Yan, X.-Q. Zhang, W.-L. Cai, J.-Q. Huang, Q. Zhang, *Angew. Chem., Int. Ed.* **2021**, *60*, 4090.
[62] C. Huang, S. X. Zhao, H. Peng, Y. H. Lin, C. W. Nan, G. Z. Cao, *J. Mater. Chem. A* **2018**, *6*, 14339.
[63] Y. Zhao, T. Zhou, T. Ashirov, M. El Kazzi, C. Cancellieri, L. P. H. Jeurgens, J. W. Choi, A. Coskun, *Nat. Commun.* **2022**, *13*, 2575.
[64] J. Liu, S. Ihuaenyi, R. Kuphal, J. Salinas, L. Xie, L. Yang, U. Janakiraman, M. E. Fortier, C. Fang, *J. Electrochem. Soc.* **2023**, *170*, 010535.
[65] T. Chen, Z. Jin, Y. Liu, X. Zhang, H. Wu, M. Li, W. Feng, Q. Zhang, C. Wang, *Angew. Chem., Int. Ed.* **2022**, *61*, 202207645.
[66] C. K. Ho, C. Y. V. Li, Z. Deng, K. Y. Chan, H. Yung, C. Yang, *Carbon N. Y.* **2019**, *145*, 614.
[67] Y. Li, K. W. Wong, Q. Dou, W. Zhang, K. M. Ng, *ACS Appl. Energy Mater.* **2018**, *1*, 2664.
[68] J. Liu, Y. Shen, L. Chen, Y. Wang, Y. Xia, *Electrochim. Acta* **2015**, *156*, 38.
[69] W. Zhang, Z. Liu, X. Xiao, D. Liu, *ChemElectroChem* **2016**, *3*, 1951.
[70] W. Qin, Y. Chen, J. An, X. Wen, *Ceram. Int.* **2022**, *48*, 22153.